Nanoscale

PAPER

View Article Online
View Journal

Cite this: DOI: 10.1039/c6nr00506c

Human immune cell targeting of protein nanoparticles – caveospheres

Joshua J. Glass,[a,b] Daniel Yuen,[c,d] James Rae,[e,f] Angus P. R. Johnston,[c,d] Robert G. Parton,[e,f] Stephen J. Kent*[a,b,g] and Robert De Rose[a,b]

Received 20th January 2016,
Accepted 22nd March 2016

DOI: 10.1039/c6nr00506c

www.rsc.org/nanoscale

Nanotechnology has the power to transform vaccine and drug delivery through protection of payloads from both metabolism and off-target effects, while facilitating specific delivery of cargo to immune cells. However, evaluation of immune cell nanoparticle targeting is conventionally restricted to monocultured cell line models. We generated human caveolin-1 nanoparticles, termed caveospheres, which were efficiently functionalized with monoclonal antibodies. Using this platform, we investigated CD4+ T cell and CD20+ B cell targeting within physiological mixtures of primary human blood immune cells using flow cytometry, imaging flow cytometry and confocal microscopy. Antibody-functionalization enhanced caveosphere binding to targeted immune cells (6.6 to 43.9-fold) within mixed populations and in the presence of protein-containing fluids. Moreover, targeting caveospheres to CCR5 enabled caveosphere internalization by non-phagocytic CD4+ T cells—an important therapeutic target for HIV treatment. This efficient and flexible system of immune cell-targeted caveosphere nanoparticles holds promise for the development of advanced immunotherapeutics and vaccines.

Introduction

The use of nanoparticles for vaccine and drug delivery enables cell-specific targeting to increase therapeutic efficiency and minimize off-target effects. Moreover, nanoparticles afford protection of unstable cargo and can facilitate entry into various immune cells.[1] Therefore, targeting nanomedicines to immune cells for use as anti-viral or anti-cancer immunotherapies holds much promise.

Monoclonal antibodies (mAb) have been hugely successful in the clinical treatment of solid and haematological cancers. Approved immunotherapies target cancer-associated antigens, such as the HER2 (trastuzumab) or CD20 (rituximab) proteins. These anti-cancer agents target cell surface receptors to (1) antagonize growth receptors required for malignant cell survival and/or (2) enhance natural killing by flagging cells for destruction,[2–4] which can include induction of antibody (Ab)-dependent cellular cytotoxicity.[5] However, harnessing the immune system using mAbs is a more recent development, by targeting immune markers such as cytotoxic T-lymphocyte-associated protein 4 (CTLA-4; ipilimumab) and programmed death 1 (PD-1; nivolumab).[6,7] These agents block inhibitory pathways on the patient's own cytotoxic T lymphocytes (CTL) to enhance natural anti-tumor immunity.[4]

Nanotechnology has the power to transform immunotherapy through protection of payloads from both metabolism and off-target effects, while enabling specific delivery of cargo to immune cells. The complex stromal environment and vascular irregularity of tumors is associated with delivery challenges for targeted nanoparticles. While tumor cell internalization of Ab-targeted nanoparticles were increased, overall localization within the tumor was not improved by targeting.[8,9] The structural hurdles associated with tumor architectures are at least partially bypassed when targeting immune cells, which are present both in the circulation and in well-vascularized immune organs.

Investigating active nanoparticle targeting in the complex environment of mixed populations of primary human blood cells has rarely been investigated. The commonly studied cell line models[10,11] ignore both non-specific association with, and competition for, large numbers of diverse cell types. We have

[a]Department of Microbiology and Immunology, Peter Doherty Institute for Infection and Immunity, The University of Melbourne, Melbourne, VIC 3010, Australia
[b]ARC Centre of Excellence in Convergent Bio-Nano Science and Technology, The University of Melbourne, Melbourne, Australia
[c]Drug Delivery, Disposition and Dynamics, Monash Institute of Pharmaceutical Sciences, Monash University, Parkville, VIC 3052, Australia
[d]ARC Centre of Excellence in Convergent Bio-Nano Science and Technology, Monash University, Parkville, Australia
[e]Institute for Molecular Bioscience and Centre for Microscopy and Microanalysis, The University of Queensland, St Lucia, QLD 4072, Australia
[f]ARC Centre of Excellence in Convergent Bio-Nano Science and Technology, The University of Queensland, St Lucia, Australia
[g]Melbourne Sexual Health Centre and Department of Infectious Diseases, Alfred Health, Central Clinical School, Monash University, Melbourne, Australia.
E-mail: skent@unimelb.edu.au

previously studied the interaction of nanoparticles in whole human blood to investigate both inhibiting the clearance of particles by phagocytic blood cells[12] and the activation of dendritic cells for vaccination purposes.[13] However, our previous studies did not utilize nanoparticle technologies capable of actively targeting specific cell populations. Employing a human blood model of primary peripheral blood mononuclear cells (PBMC), we now investigate the effect of Ab-functionalization on the delivery of caveolin cage nanoparticles—termed h-caveolae or 'caveospheres'—to CD4+ T cells and B cells.

One acquired disorder of the immune system is HIV-1 infection, which causes destruction of CD4+ T cells leading to AIDS. HIV-1 lies dormant in resting CD4+ T cells despite current therapies, rendering it incurable. Targeting CD4+ T cells with nanoparticles might be used to either enhance T cell immunity or to deliver nanoparticle HIV-1 therapeutics, since CD4+ T cells are the primary target for HIV-1 infection. A critical challenge of delivering nanoparticles into CD4+ T cells arises due to their non-phagocytic nature. In primary T cells, the CD4 cell surface molecule displays negligible internalization when targeted by mAbs[14,15] and is unlikely to lead to efficient nanoparticle internalization. In contrast, C–C chemokine receptor type 5 (CCR5) displays rapid internalization kinetics.[16,17] CCR5 is a chemokine receptor present on memory CD4+ T cells[18] and serves as a co-receptor for the majority of HIV-1 strains.[19] As such, targeting nanoparticles to CCR5+ CD4+ T cells represents an approach towards targeting anti-HIV therapeutics to the primary cell target of HIV-1 infection.

Caveolae are 50–80 nm membrane pits that are naturally found in a variety of mammalian cell types.[20] Caveolins are the major membrane proteins of caveolae, which form important endocytic vesicles and function as plasma membrane sensors.[21,22] Recently, however, the ability of human caveolin proteins to form vesicles has been exploited. By expressing recombinant human caveolin-1 in *E. coli*, caveosphere vesicles of 45–50 nm could be produced and purified.[23] Caveospheres represent genetically encoded protein–lipid vesicles that can be loaded with therapeutics and their surface modified with proteins by the expression of caveolin-fusion proteins. Our previous work has demonstrated this model holds promise for targeted delivery of caveospheres into the human SK-BR-3 breast cancer cell line.[23]

Herein we generate and evaluate a versatile caveosphere platform that can be rapidly functionalized with monoclonal Abs. We show that caveospheres can actively target primary human immune cells within mixed blood cell populations and can be internalized by non-phagocytic primary immune cells. This targeting model is more relevant and sensitive than cell line models, demonstrating enhanced non-specific binding.

Experimental

Nanoparticle preparation

Caveosphere nanoparticles expressing a minimal IgG Fc-binding Z-domain[24] of Protein A were produced as per Walser *et al.*[23] Briefly, *E. coli* (Rosetta pLysS DE3) were grown in Terrific Broth at 37 °C to an OD600 nm of 1. Bacteria were induced to express the recombinant caveolin-1 fusion protein by addition of 1 mM IPTG (Astral Scientific). Cells were cultured overnight at 30 °C, pelleted, resuspended in high salt PBS (300 mM NaCl; pH 7.4) with protease inhibitors then lysed using a cell disruptor (Constant Systems). The resultant mixture was spun at high speed (20 000*g*) to remove cellular debris and the supernatant was poured into an Amylose resin (NEB) column for purification by affinity chromatography. The resulting particles were eluted with maltose (10 mM) then concentrated using Amicon Ultra-15 100 kDa MWCO (Merck Millipore). Post-purification, caveospheres were fluorescently labelled using Alexa Fluor 647 succinimidyl ester (Thermo Fisher). Unreacted dye removed by centrifugal ultrafiltration using Amicon Ultra-4 100 kDa MWCO (Merck Millipore).

Ab functionalization

Caveospheres were incubated with purified mouse anti-human IgG Ab for at least 24 h at 4 °C. Ab was added at a 1 : 2 mass ratio with nanoparticles, providing an Ab functionalization of approximately 10% of available nanoparticle Ab-binding sites; this equates to an estimated average of 16.4 Abs per particle (data not shown). Targeting Abs were CD4 (OKT4, Ms IgG2b, BioLegend), CD20 (2H7, Ms IgG2b, BioLegend) and CCR5/CD195 (3A9, Ms IgG2a, BD Biosciences).

Nanoparticle characterization

Ab functionalization was confirmed after incubating with polystyrene microbeads coated with or without anti-mouse κ light chain IgG (BD Biosciences) for 15 min and washing with 1× PBS. Using flow cytometry (BD LSR Fortessa), beads were gated by FSC/SSC and AF647 signals analyzed.

Negative staining electron microscopy was performed as follows. Purified caveospheres were incubated for 10 minutes with glow-discharged and carbon-coated 1% formvar support film on a 200 mesh Cu grid (ProSciTech). Caveospheres were washed 5 times in water then stained with 1% aqueous uranyl acetate. Imaging was performed on a JEOL 1011 electron microscope at 80 kV fitted with a Morada 4k × 4k soft imaging camera (Olympus) with 2-fold binning. Caveosphere size was determined by measuring the diameter of 100 caveospheres/sample (Fiji v.2.0). Nanoparticle size was also examined by dynamic light scattering, using a Nanopartica SZ-100 (Horiba Scientific).

Cells

The CD4+ T cell line CEM.NKR-CCR5 (NIH AIDS Reagent Program) and CD20+ B cell line 721.221 (kindly donated by Andrew Brooks, Melbourne, Australia) were maintained in RF10 [RPMI 1640 (Life Technologies), supplemented with 10% fetal calf serum (Gibo, Life Technologies), and L-glutamine, penicillin and streptomycin (500 μg ml^{-1}, Gibco, Life Technologies)].

Blood was collected from healthy donors into sodium heparin vacuettes (Greiner Bio-one) after obtaining informed

consent in accordance with University of Melbourne approved protocols. Peripheral blood mononuclear cells (PBMC) were purified by density gradient centrifugation using Ficoll-Paque PLUS (GE Healthcare). For nanoparticle internalization experiments, PBMC were enriched for CD4+ T cells to a purity >97% by negative magnetic cell selection (Stem Cell Technologies).

Cell line targeting

Cells were harvested and resuspended at a density of 10^6 cells per 100 μl in RF10. Cells were incubated with 1 μg nanoparticle for 1 h on ice, washed twice and fixed on ice with 1% formaldehyde. Nanoparticle–cell interactions assessed after gating on single cells and analysing AF647 signals by flow cytometry (BD LSR Fortessa) or imaging flow cytometry (Amnis ImageStream). Cell expression of CD4 and CD20 were evaluated by flow cytometry after phenotyping with optimized concentrations of CD4 (AF488, OKKT4, BD Biosciences) and CD20 (BV421, 2H7, BD Biosciences) for 1 h on ice.

Targeting in mixed blood populations

PBMC were washed in FACS wash buffer (FWB; 1× PBS containing 0.5% w/v bovine serum albumin (Sigma Aldrich) and 2 mM EDTA pH 8 (Ambion)) and phenotyped on ice (1 h) in the presence of Brilliant Stain Buffer (BD Biosciences) using titrated concentrations of antibodies against CD3 (AF488, SP34-2, BD Biosciences), CD8 (BV570, RPA-T8, BioLegend), CD14 (PE-Cy7, M5E2, BD Biosciences), CD19 (BV650, HIB19, BioLegend), CD45 (V500, HI30, BD Biosciences) and CD56 (PE, NCAM16.2, BD Biosciences). Cells washed twice in FWB and resuspended at 10^6 cells per 100 μl in 5 mL polystyrene round-bottom tubes ('FACS tubes'; Falcon). Nanoparticles (1 μg) added and incubated on ice for 1 h. Cells washed, fixed (1% formaldehyde) and analysed by flow cytometry (LSRFortessa, BD Biosciences). For confocal microscopy, cell types of interest were sorted using the same antibody panel and a BD FACS ARIA III (100 μm nozzle). Sorted cells were washed twice before mounting and imaging as below (See Confocal microscopy).

Nanoparticle internalization

CEM.NKR-CCR5 or primary CD4+ T cells were seeded into FACS tubes at 10^6 per 100 μl in RF10, incubated at 37 °C or on ice for 15 min, before adding 1 μg untargeted or αCCR5-functionalized caveospheres for 90 min. Cells washed in PBS, membranes stained with CD4-FITC or -AF488 (BD Biosciences) and washed twice more.

Confocal microscopy

Coverslips (# 1.5, Menzel-Glaser) treated with poly-L-lysine (Sigma Aldrich) for 2 h, room temp. (RT), washed thrice with 1× PBS and allowed to dry. Cells (100 μl) added to coverslips and allowed to set for 1 h, RT, and fixed with 1% formaldehyde. Cells rinsed twice in PBS, stained with DAPI (10 μg ml^{-1}, Thermo Fisher), rinsed twice and mounted onto glass slides using ProLong Diamond Antifade (Thermo Fisher).

Cells imaged by confocal microscopy using 20× and 63× oil objectives (Zeiss LSM710 and ZEN 2012 Black software), and 3D renders generated using Imaris 7 (Bitplane). Nanoparticle–cell interactions (association and internalization) were quantitated using ZEN Lite 2012, by stepping through *z*-stacks and counting the percentage of cells containing AF647-labelled nanoparticles at the surface or inside (>100 cells per condition).

Statistical analyses

Results analysed using non-parametric one-way ANOVA (Friedman test) followed by Dunn's multiple comparisons test (GraphPad Prism 6).

Results

Generation of immune cell targeted caveospheres

We have previously shown that caveosphere assembly can tolerate the presence of foreign proteins fused to caveolin-1[23] without substantial impact upon nanoparticle yield. To facilitate a flexible Ab-mediated targeting system, caveolin-1 was engineered to display the minimal 'Z-domain' of the Staphylococcal Fc-binding Protein A (Fig. 1A). Expression of mammalian caveolin-1 in *E. coli* results in insertion of the recombinant protein into the bacterial cytoplasmic membrane, inducing membrane curvature and invagination of the bacterial inner membrane. Importantly, the insertion of the hairpin intramembrane domain positions both N and C termini of caveolin-1 on the 'outer' surface of the resulting caveosphere, presenting both the Z-domain and affinity purification tag on the surface of the nanoparticle (Fig. 1B).

To characterize Ab functionalized Z-domain-bearing caveospheres, we incubated AF647-labelled Z-domain-bearing caveospheres with αCD4 and αCD20 IgG Abs (which target CD4+ T cells and B cells, respectively). We used electron microscopy to examine the morphology of caveospheres (Fig. 2A). The spherical nature and hollow internal architecture (as evidenced by biconcave electron densities) remain following Ab functionalization. By EM, no significant alteration in diameter was observed following Ab-functionalization (Fig. 2B). Untargeted caveospheres measured 42.7 ± 8.3 nm, while αCD4- and αCD20-functionalized caveospheres were 41.3 ± 8.3 and 45.3 ± 6.8 nm, respectively (Fig. 2A). By DLS, the hydrodynamic radii of untargeted caveospheres measured 70.1 ± 18.7 nm, αCD4-caveospheres 62.1 ± 15.9 nm and αCD20-caveospheres 61.2 ± 19.8 nm (Fig. 2B). The increased average size measured by DLS likely reflects the size of the water shell surrounding the nanoparticles rather than their electron densities.

The capacity of caveospheres to bind Ab at their surface was next assessed by flow cytometry (Fig. 2C). We incubated fluorescently labelled caveospheres with polystyrene microbeads functionalized with anti-κ light chain Abs on their surface. These 'Ab-capture' microbeads will bind caveospheres if targeting Abs have bound the caveosphere surface, while control microbeads coated with bovine serum albumin (BSA) only will

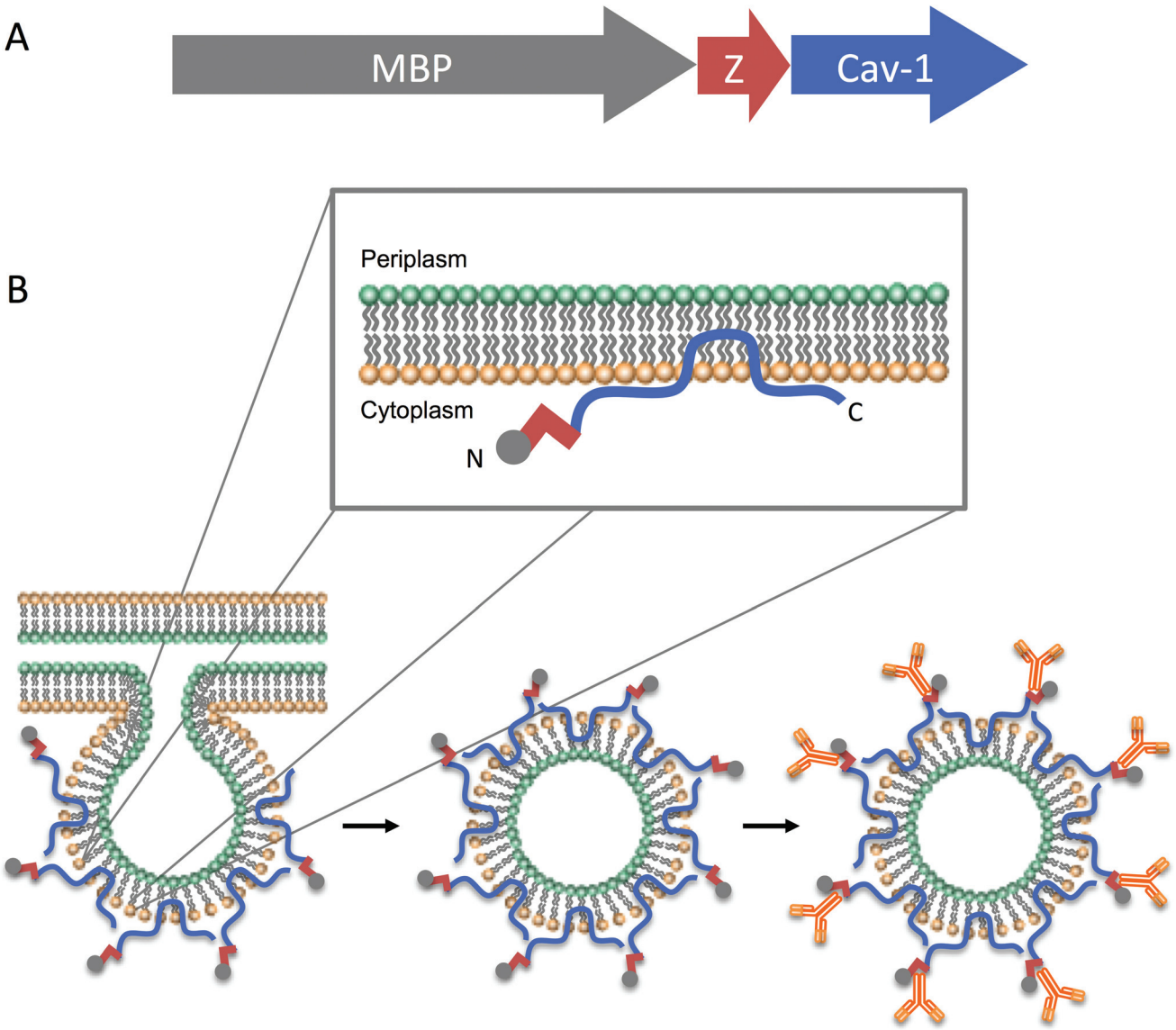

Fig. 1 Schematic of 'Z-domain' containing caveospheres. (A) Caveosphere monomers comprise a caveolin-1 (cav-1) subunit with a maltose-binding protein (MBP) and Z-domain at the N-terminus. (B) (Inset) Cav-1 (blue) inserts into the bacterial inner membrane, with N- and C-termini in the cytoplasm. The Z-domain (red) binds to the Fc region of IgG, while MBP (gray) allows purification and aids stability. MBP-Z-Cav1 monomers invaginate from the bacterial inner membrane to form 'caveospheres' that bud into the cytoplasm. Following bacterial lysis, caveospheres are purified and post-functionalized with IgG (orange). Schematic not to scale.

not bind Ab (and hence neither targeted nor untargeted caveospheres). After washing away free caveospheres, the fluorescent caveosphere signal attached to microbeads was analyzed by flow cytometry. Ab-capture, but not control, microbeads incubated with αCD4- and αCD20-caveospheres produced strong fluorescence, indicating Ab on the caveosphere surface. Importantly, since the anti-κ light chain Ab on the positive microbead binds the antigen-binding end of Abs, this assay suggests that caveosphere surface Abs are in the correct orientation for cell targeting. A small binding artefact of untargeted (non-functionalized) caveospheres to Ab-capture microbeads may represent caveosphere Z-domains weakly binding the microbead's own surface Ab.

Binding of Ab-functionalized caveopheres to CD4+ T cell and B cell lines

In preparation for studies in the more complex environment of human blood cells, we first assessed binding of αCD4 and αCD20 Ab-functionalized caveospheres to T and B cell lines suspended in RF10. The two cell lines chosen, CEM.NKR-CCR5 and 721.221, express either CD4 or CD20 respectively (Fig. 3A), therefore providing additional controls for caveosphere binding. By standard flow cytometry, we observed targeted binding of αCD4 caveospheres to CEM.NKR-CCR5 (80.4 ± 0.1%) and αCD20 caveospheres to 721.221 (57.6 ± 0.5%, Fig. 3B). There was very low non-specific association of either untargeted or

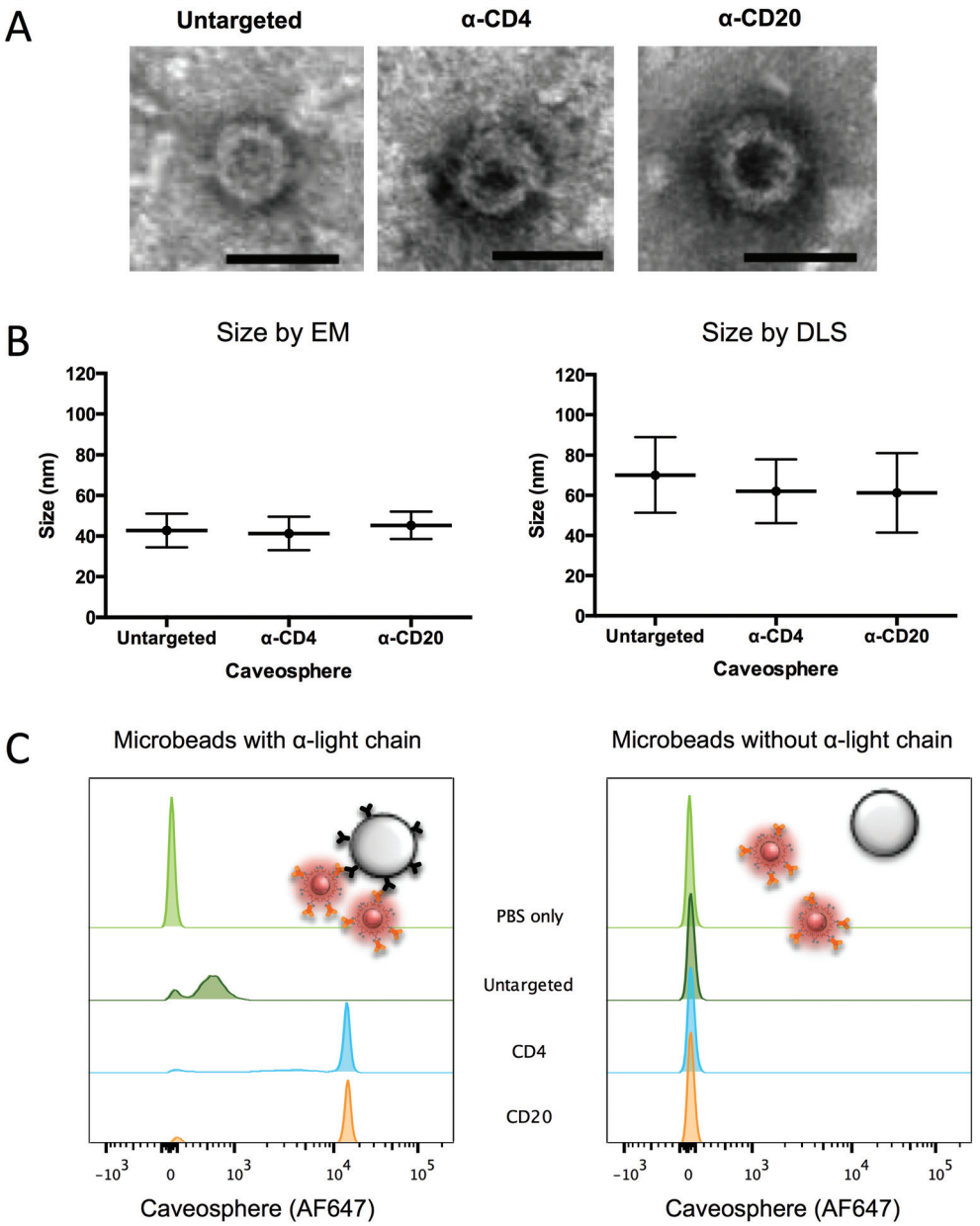

Fig. 2 Characterization of 'Z-domain' containing caveospheres. (A) Caveospheres were imaged by negative stain electron microscopy. Their spherical morphology is unchanged after Ab functionalization. Scale bar = 50 nm. (B) (Left) Caveosphere diameters were measured by electron microscopy (100 caveospheres per sample). (Right) Caveosphere size was analyzed by DLS. Samples run 2–3 times, with mean and SD of each run averaged. (B) Caveospheres (red spheres) were incubated with Ab-capture microbeads (gray spheres) functionalized with anti-κ light chain Abs on their surface. Control microbeads were coated with bovine serum albumin. Therefore, anti-light chain but not control microbeads will bind Ab-functionalized nanoparticles. After gating on microbeads by flow cytometry (FSC/SSC), AF647 signals associated with caveospheres were examined.

'off-targeted' caveospheres to CEM.NKR-CCR5 and 721.221 (<1% and <2%, respectively). To confirm targeted binding and to visualize particle density and location, we employed imaging flow cytometry (Fig. 3C). Again we observed high levels of association of CD4- and CD20-targeted caveospheres to the relevant cell lines (71.0 and 50.0%, respectively). Interestingly, αCD4-caveospheres that bound CEM.NKR cells consistently displayed punctate association patterns while αCD20-caveopsheres bound 721.221 cells more diffusely (Fig. 3C, left).

Specific binding of Ab-functionalized caveospheres to CD4+ T cells and B cells within human PBMCs

Analysis of nanoparticle association with cell lines does not mimic the complexity of multiple sub-populations within human tissues such as blood. We therefore isolated PBMC from the fresh blood of nine healthy human donors, identified cell populations using fluorescent Abs and examined the targeting of caveospheres to different cell populations.

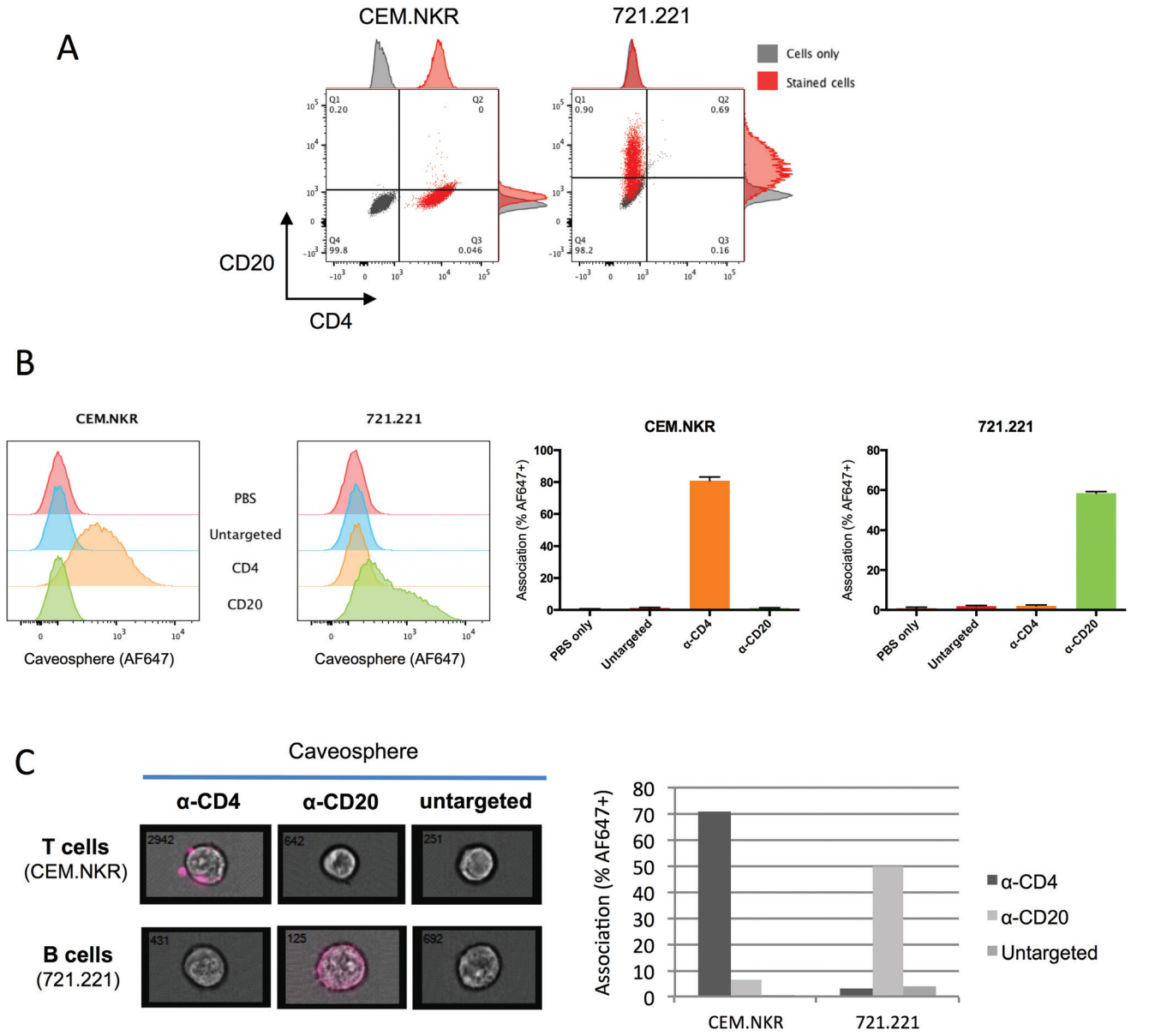

Fig. 3 Caveospheres can be targeted to immune cells based on expression of surface proteins. (A) Cell lines were examined for their expression of the T cell marker CD4 or B cell marker CD20 by flow cytometry. (B) Targeting of mouse anti-human IgG2b-functionalized caveospheres to CEM.NKR and 721.221 cells was examined by flow cytometry. (Left) Representative histograms are shown. (Right) The association of targeted caveospheres with cells is plotted, with mean and SD from 3 independent assays. 30 000 cells were collected per sample. (C) Targeting was confirmed by imaging flow cytometry. 3000 cells per condition were imaged and only in-focus cells analysed. (Left) Representative images selected, showing cells (brightfield) and caveospheres (magenta). (Right) Association by imaging flow cytometry was quantitated.

Using flow cytometry and an optimized panel of 6 fluorescent Abs, we studied gated populations of 4 cell populations for association with untargeted, CD4- and CD20-targeted caveospheres: CD4+ T cells, CD19+ B cells, NK cells and monocytes (Fig. 4A). A clear preference for CD4- and CD20-targeted caveospheres to associate with CD4+ T cells and B cells, respectively, was observed (Fig. 4B and C). αCD4-caveospheres bound 76.0 ± 11.3% of CD4+ T cells, while αCD20-caveospheres bound 79.3 ± 23.6% of B cells. The sensitivity of this system resulted in higher background association with all cell types, which was not captured when examining targeting in cell lines (Fig. 3). However, the effect of targeting was clearly demonstrated by fluorescence intensity. Compared with untargeted nanoparticles, the median caveosphere fluorescence (MFI) per CD4+ T cell was 43.9 ± 12.7 fold greater with αCD4-caveospheres, while MFI per B cell was 6.6 ± 1.0 fold greater with αCD20-caveospheres (Fig. 4C).

Both untargeted and CD4-targeted particles bound primary B cells (48.3 ± 13.0% and 51.6 ± 10.6%, respectively), although the intensity of binding was less than that for αCD20-caveo-

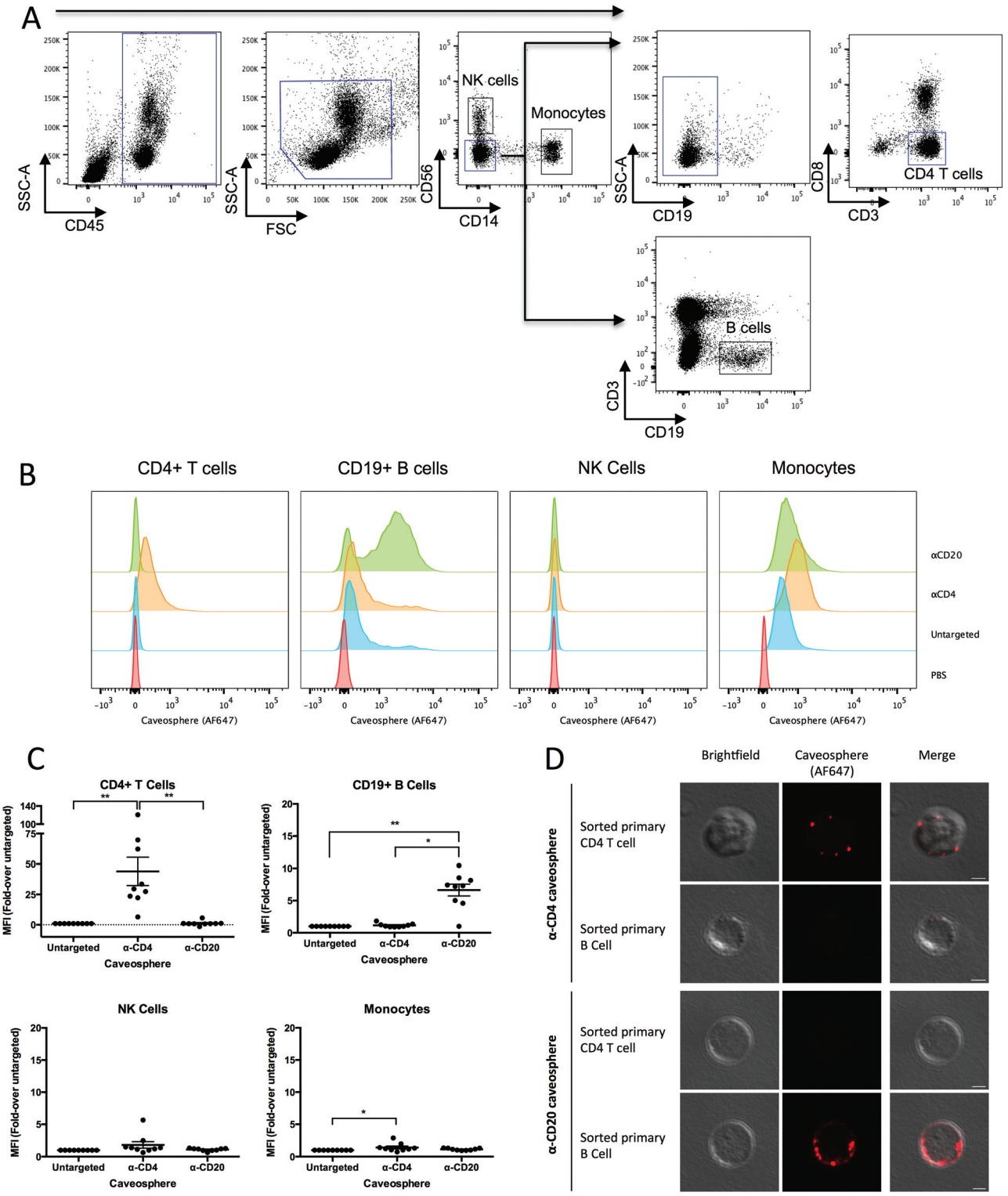

Fig. 4 Caveospheres can be targeted to primary B and T cells within mixed human blood cell populations. PBMC were purified from healthy donors, phenotyped using a 6-antibody cocktail and incubated with caveospheres functionalized with or without anti-human Abs. (A) Gating strategy used to identify leukocyte populations. After gating on final populations, single cells were selected by FSC-A *vs.* FSC-H. (B) Targeting was examined in primary human PBMCs. Representative FACS plots from one donor showing caveosphere binding to cell subsets. (C) Binding is displayed as fold change of MFI over untargeted caveosphere, with mean ± SEM. $n = 9$ donors across independent experiments. * $p < 0.05$, ** $p < 0.01$. (D) Confocal microscopy of sorted primary immune cells confirmed the targeting of α-CD4 and α-CD20 caveospheres. Representative images displayed, showing brightfield and caveospheres (red). Scale bar = 2 μm.

spheres. As B cells display Ab on their surface, and our particles had approximately 90% of the Ab-binding Z-domains left unfunctionalized, this background binding may represent the association of free Z-domains with Fc regions of B cell surface Ab. The control population of NK cells do not express Ab, nor CD4 or CD20 surface molecules and exhibited lower association with all caveospheres. Although the number of caveospheres associating with NK cells (indicated by MFI) was substantially lower than to targeted cell types (Fig. 4B), caveospheres still associated with NK cells from most donors (28.8 ± 25.1%) albeit at very low levels per cell. Monocytes are highly adapted to associate with nanoparticles (Fig. 4B), although there was minimal change in association comparing untargeted and targeted caveospheres (Fig. 4C). A small but statistically significant increase in the association of monocytes with αCD4-caveospheres is consistent with low CD4 expression on monocytes.[18]

Using confocal microscopy on sorted CD4 T cells and B cells, we confirmed selective targeting of CD4 T cells (and not B cells) by αCD4-caveospheres and selective targeting of B cells (and not CD4 T cells) by αCD20-caveospheres (Fig. 4D).

Uptake and internalization of CCR5 targeted caveospheres into CD4+ T cells

To use nanoparticles for delivering HIV therapeutics inside CD4+ T cells, we need to achieve nanoparticle endocytosis. We therefore generated caveospheres functionalized with αCCR5 Ab, since this is the co-receptor used by most strains of HIV-1 to enter cells. We first confirmed the presence of surface Ab by flow cytometry using Ab-capture microbeads (as in Fig. 1D,

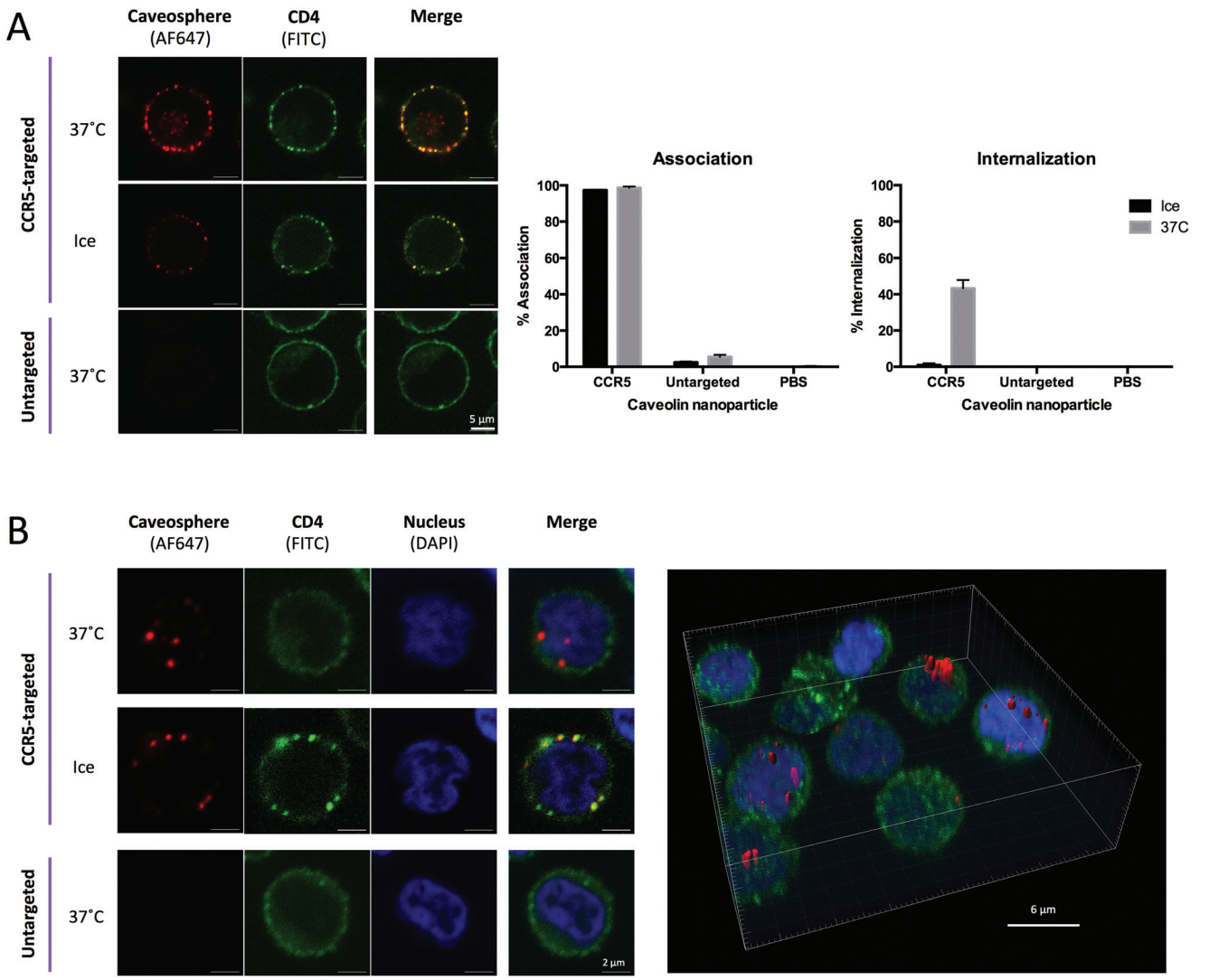

Fig. 5 Caveospheres are internalized by T cells in the presence of serum proteins after targeting CCR5. (A) Internalization into CEM.NKR-CCR5 cells. CCR5-targeted but not untargeted caveospheres are internalized at 37 °C. (Left) Middle slice of representative cells by confocal microscopy. (Right) Targeting efficiency was calculated by quantitating confocal microscopy images and displayed as % association and % internalization, with mean ± SEM of 3 independent experiments displayed (>100 cells per condition). (B) Internalization into primary CD4 T cells. (Left) Middle slice of representative cells. (Right) Representative field of view showing caveospheres internalized by primary CD4 T cells from 2 independent experiments (>100 cells per condition). Scale bars: A. 5 µm, B. 2 µm, C. 6 µm.

data not shown). To investigate internalization, we employed confocal microscopy. The CEM.NKR-CCR5 CD4+ T cell line stably expresses the CCR5 receptor and was selected for initial investigations. Cells were incubated with CCR5-targeted or untargeted caveospheres in serum-containing media for 90 min on ice or at 37 °C, before staining the cell membranes with αCD4 IgG. Multiple *z*-stacks were imaged to examine the presence of fluorescent-caveospheres on the surface or within cells (Fig. 5A). As CCR5 internalization is an active, receptor-mediated process, incubations on ice control for passive, non-specific nanoparticle entry. Moreover, incubations with untargeted caveospheres control for CCR5-independent internalization of nanoparticles. We observed αCCR5-caveospheres associating with cells on ice and at 37 °C, with association/cell elevated at 37 °C (Fig. 5A, left).

Targeted but not untargeted caveospheres were internalized at 37 °C (Fig. 5A, left). Cell association and internalization of caveospheres were quantitated after viewing *z*-stacks for >100 cells per condition (Fig. 5A, right). αCCR5-caveospheres associated with almost all of the CD4+ CCR5+ T cells at 37 °C (98.6 ± 0.7%) and on ice (97.4 ± 0.2%), while untargeted particles associated with only 5.4 ± 1.2% (37 °C) and 2.5 ± 0.4% (ice) of cells. Internalization was reasonably efficient, with 43.3 ± 4.6% of cells internalizing αCCR5-caveospheres at 37 °C. Targeted internalization was dramatically abrogated on ice (0.98 ± 0.98%), while untargeted caveospheres never entered cells. Due to the presence of unoccupied Z-domains, post-labelling cells with αCD4-FITC will also bind surface-bound, but not internalized, caveospheres. Therefore, surface bound caveospheres co-localize with FITC and provide an additional internalization control. Taken together, these results suggest a receptor-mediated, active endocytosis mediating the uptake of CCR5-targeted caveospheres.

While the CCR5-transduced CEM.NKR T cell line internalized targeted caveospheres efficiently, they remain only a model of primary human CD4+ T cells. Therefore, PBMCs were obtained from the fresh blood of healthy donors and CD4+ T cells purified by negative magnetic depletion. Peripheral blood CCR5+ CD4+ T cells represent a stable cell population able to be infected by the majority of HIV-1 strains. Untargeted and CCR5-targeted caveospheres were incubated with CD4+ T cells at 37 °C and on ice. As with the CCR5-transduced cell line, we observed a temperature- and receptor-mediated active endocytosis of caveospheres (Fig. 5B, left). αCCR5-caveospheres bound the surface of cells at each temperature, and at 37 °C were internalized by up to 34% of CD4+ T cells (data not shown). Untargeted caveospheres never entered cells. A representative field of view (Fig. 5B) demonstrates the range in quantity and location of internalized αCCR5-caveospheres per cell.

Discussion

The use of targeted nanoparticles for disease treatment and prevention holds much promise and is receiving increasing attention.[1,25] However, most studies examine targeting in monocultured cell line models that lack the complexities of true human systems such as blood. Caveospheres represent versatile protein–lipid nanoparticles that can be rapidly functionalized with Ab. Using this nanoparticle platform we demonstrated targeting to primary human immune cells within mixed blood cell populations. Moreover, targeting caveospheres enables their internalization by therapeutically relevant, non-phagocytic immune cells.

Multi-cell systems, such as the primary human PBMC model presented herein, provide additional controls and biological relevance compared with examining targeting in monocultures of transformed cell lines. PBMCs allow evaluation of the balance between nanoparticle targeting and non-specific association, including competition with control populations in a physiologically relevant cell mixture. As shown here, such non-specific association can be low (NK cells) or high (monocytes). Moreover, primary human cells are more therapeutically relevant targets than transformed cell lines that often contain altered cell surface phenotypes and cannot reflect inter-donor variability.

When a nanoparticle is transferred into a biological environment, a dynamic protein corona forms on the nanoparticle surface that evolves as it traverses biological fluids (*e.g.* from plasma into the cytosol).[26] Targeting cells in the presence of serum is required for the systemic administration of nanomedicines. However, studies report differing abilities to target in the presence of protein coronas. Recently, Dai *et al.*[10] examined targeting in the context of increasing concentrations of serum and found that protein corona formation did not significantly alter the targeting ability of Ab-functionalized layer-by-layer polymer particles or capsules. In contrast, other groups have demonstrated a reduction in nanoparticle targeting in serum-containing *vs.* serum-free media.[27–29] For example, the uptake of transferrin-functionalized nanoparticles by A549 cells is substantially reduced in as little as 10% FCS.[28] Our studies of this caveosphere system were performed in the presence of 10% v/v fetal bovine serum or 0.5% w/v bovine serum albumin, likely generating a significant protein corona. Despite this, we were able to efficiently target and achieve internalization of appropriately targeted caveospheres to cell lines and primary immune cells. Further analysis of the protein corona formed on caveospheres in the presence of targeting surface mAbs might reveal insights that could further enhance immune cell targeting.

Achieving nanoparticle internalization by CD4+ T cells offers the possibility of targeted immunotherapy for diseases such as HIV-1, which is characterized by infection of this cell type. Previous studies have investigated nanoparticle internalization into CD4+ T cells. Mouse splenic T cells were shown by confocal microscopy to internalize HIV-1 Tat-functionalized superparamagnetic iron oxide nanoparticles following an 18 hour incubation.[30] However, Tat results in non-specific cargo delivery[31–33] and these small (5 nm) nanoparticles were unsuitable for cargo delivery. In an attempt to restrict targeting to T cells, Dinauer *et al.*[34] functionalized 211 nm gelatin

nanoparticles with Ab targeting the pan-T cell marker CD3. Primary peripheral blood lymphocytes were cultured for 7 days, then enriched for T cells by stimulating with phytohemagglutinin and culturing in IL-2. Nanoparticles were internalized by the cultured T cell population following a 4 h incubation. In contrast, we restricted nanoparticle targeting to CCR5+ cells, which comprise just 2–3% of total circulating T cells and are largely of the memory phenotype.[35] We demonstrated internalization of CCR5-targeted caveospheres by fresh human CD4+ T cells after just 90 min. To our knowledge, this is the first report of CCR5-targeting of nanoparticles to induce internalization into CD4+ T cells.

Caveospheres can incorporate therapeutics in their hollow core[23] and may facilitate novel HIV-1 therapeutic strategies. For example, HIV-1 is not curable with current drug therapies as latent provirus can remain dormant in CCR5+ CD4+ T cells. HIV-1 silencing RNAs[36,37] could be packaged into targeted caveospheres to avert serum nucleases and allow delivery into CCR5+ CD4+ T cells to force the maintenance of viral latency and prevent the recrudescence of HIV-1 infection when anti-HIV drugs are ceased. Alternatively, latency-reactivating agents, such as histone deacetylase inhibitors,[38] which purge latently infected cells to express viral proteins and become visible to the immune system could be encapsulated and targeted to improve their safety profile by restricting their cell uptake. Caveospheres can be loaded with small molecules able to pass through the bacterial outer membrane during caveosphere expression, therefore entering the periplasmic space and becoming incorporated into the caveosphere core. However, to load larger molecules such as proteins or RNA, caveosphere production may require cell-free protein expression systems.

Research into the field of 'nanovaccinology' is rapidly expanding.[1,25,39] This caveosphere platform allows surface display of antigen by manipulating the C-termini of caveolin monomers (unpublished data). Herein we have demonstrated targeting to common primary immune cells, warranting investigation of targeting to more scarce dendritic cell populations. Targeting dendritic cell receptors represents a potent vaccine approach, by activating both the humoral and cellular arms of the immune system.[40,41] We are currently investigating the generation of DC-targeted antigen-expressing caveospheres to induce robust immune responses.

Our caveosphere platform allows rapid functionalization with different targeting Abs. This is highly suited for *in vitro* or *ex vivo* investigation. Although we demonstrated targeting in the presence of bovine serum IgG, the high concentration of IgG (with strong affinity to Protein A) in human blood might compete off targeting IgG and render this system less suitable *in vivo*. We have previously generated caveospheres expressing single chain fragment variable (scFv) domains[23] and are actively investigating chemical conjugation of IgG, which are better suited to future *in vivo* studies. By nature of their bacterial origin, caveospheres contain immunostimulatory molecules. Delivering anti-HIV-1 therapeutics will require non-immunstimulatory caveospheres and efforts are underway to overcome this potential problem.

Conclusion

Using caveosphere nanoparticles, we have demonstrated targeting to primary human immune cells, including internalization by non-phagocytic CD4+ T cells, in the presence of serum proteins. We believe the investigation of nanoparticle targeting in mixed primary blood cells is more rigorous than targeting mono-cultured transformed cell lines. Primary blood cells express physiological levels of targeted surface receptors, while providing additional off-target control populations and competition from multiple cell types. Lastly, CCR5-targeted nanoparticles represent a potential strategy for delivering anti-HIV therapeutics that warrants further investigation.

Acknowledgements

We thank Ms Sheilajen Alcantara and Ms Thakshila Amarasena for their technical assistance and advice. The authors acknowledge the facilities, and the scientific and technical assistance, of the Biological Optical Microscopy Platform, The University of Melbourne, and the Australian Microscopy & Microanalysis Research Facility at the Centre for Microscopy and Microanalysis, The University of Queensland. Research was supported by the Australian Research Council Centre of Excellence in Convergent Bio-Nano Science and Technology.

References

1 D. J. Irvine, M. C. Hanson, K. Rakhra and T. Tokatlian, *Chem. Rev.*, 2015, **115**, 11109–11146.
2 D. J. Slamon, B. Leyland-Jones, S. Shak, H. Fuchs, V. Paton, A. Bajamonde, T. Fleming, W. Eiermann, J. Wolter and M. Pegram, *N Engl. J. Med.*, 2001, **344**, 783–792.
3 R. Ramakrishnan, D. Assudani, S. Nagaraj, T. Hunter, H.-I. Cho, S. Antonia, S. Altiok, E. Celis and D. I. Gabrilovich, *J. Clin. Invest.*, 2010, **120**, 1111.
4 A. Ribas, *N Engl. J. Med.*, 2012, **366**, 2517–2519.
5 J. Du, S. Lopez-Verges, B. N. Pitcher, J. Johnson, S.-H. Jung, L. Zhou, K. Hsu, M. S. Czuczman, B. Cheson and L. Kaplan, *Cancer Immunol. Res.*, 2014, **2**(9), 878–889.
6 I. Mellman, G. Coukos and G. Dranoff, *Nature*, 2011, **480**, 480–489.
7 S. L. Topalian, F. S. Hodi, J. R. Brahmer, S. N. Gettinger, D. C. Smith, D. F. McDermott, J. D. Powderly, R. D. Carvajal, J. A. Sosman, M. B. Atkins, P. D. Leming, D. R. Spigel, S. J. Antonia, L. Horn, C. G. Drake, D. M. Pardoll, L. Chen, W. H. Sharfman, R. A. Anders, J. M. Taube, T. L. McMiller, H. Xu, A. J. Korman, M. Jure-Kunkel, S. Agrawal, D. McDonald, G. D. Kollia, A. Gupta, J. M. Wigginton and M. Sznol, *N Engl. J. Med.*, 2012, **366**, 2443–2454.
8 D. B. Kirpotin, D. C. Drummond, Y. Shao, M. R. Shalaby, K. Hong, U. B. Nielsen, J. D. Marks, C. C. Benz and J. W. Park, *Cancer Res.*, 2006, **66**, 6732–6740.

9 H. Hatakeyama, H. Akita, E. Ishida, K. Hashimoto, H. Kobayashi, T. Aoki, J. Yasuda, K. Obata, H. Kikuchi and T. Ishida, *Int. J. Pharm.*, 2007, **342**, 194–200.
10 Q. Dai, Y. Yan, C.-S. Ang, K. Kempe, M. M. Kamphuis, S. J. Dodds and F. Caruso, *ACS Nano*, 2015, **9**, 2876–2885.
11 K. Zarschler, K. Prapainop, E. Mahon, L. Rocks, M. Bramini, P. Kelly, H. Stephan and K. Dawson, *Nanoscale*, 2014, **6**, 6046–6056.
12 J. Cui, R. De Rose, K. Alt, S. Alcantara, B. M. Paterson, K. Liang, M. Hu, J. J. Richardson, Y. Yan, C. M. Jeffery, R. I. Price, K. Peter, C. E. Hagemeyer, P. S. Donnelly, S. J. Kent and F. Caruso, *ACS Nano*, 2015, **9**, 1571–1580.
13 R. De Rose, A. N. Zelikin, A. P. Johnston, A. Sexton, S.-F. Chong, C. Cortez, W. Mulholland, F. Caruso and S. J. Kent, *Adv. Mater.*, 2008, **20**, 4698–4703.
14 A. Pelchen-Matthews, J. E. Armes, G. Griffiths and M. Marsh, *J. Exp. Med.*, 1991, **173**, 575–587.
15 A. Khaled, S. Guo, F. Li and P. Guo, *Nano Lett.*, 2005, **5**, 1797–1808.
16 A. Amara, S. Le Gall, O. Schwartz, J. Salamero, M. Montes, P. Loetscher, M. Baggiolini, J.-L. Virelizier and F. Arenzana-Seisdedos, *J. Exp. Med.*, 1997, **186**, 139–146.
17 M. Mack, B. Luckow, P. J. Nelson, J. Cihak, G. Simmons, P. R. Clapham, N. Signoret, M. Marsh, M. Stangassinger and F. Borlat, *J. Exp. Med.*, 1998, **187**, 1215–1224.
18 B. Lee, M. Sharron, L. J. Montaner, D. Weissman and R. W. Doms, *Proc. Natl. Acad. Sci. U. S. A.*, 1999, **96**, 5215–5220.
19 B. F. Keele, E. E. Giorgi, J. F. Salazar-Gonzalez, J. M. Decker, K. T. Pham, M. G. Salazar, C. Sun, T. Grayson, S. Wang and H. Li, *Proc. Natl. Acad. Sci. U. S. A.*, 2008, **105**, 7552–7557.
20 N. Ariotti, J. Rae, N. Leneva, C. Ferguson, D. Loo, S. Okano, M. M. Hill, P. Walser, B. M. Collins and R. G. Parton, *J. Biol. Chem.*, 2015, **290**, 24875–24890.
21 R. G. Parton and K. Simons, *Nat. Rev. Mol. Cell Biol.*, 2007, **8**, 185–194.
22 R. G. Parton and M. A. del Pozo, *Nat. Rev. Mol. Cell Biol.*, 2013, **14**, 98–112.
23 P. J. Walser, N. Ariotti, M. Howes, C. Ferguson, R. Webb, D. Schwudke, N. Leneva, K.-J. Cho, L. Cooper and J. Rae, *Cell*, 2012, **150**, 752–763.
24 A. C. Braisted and J. A. Wells, *Proc. Natl. Acad. Sci. U. S. A.*, 1996, **93**, 5688–5692.
25 J. J. Glass, S. J. Kent and R. De Rose, *Expert Rev. Vaccines*, 2016, DOI: 10.1586/14760584.2016.1141054.
26 M. Lundqvist, J. Stigler, T. Cedervall, T. Berggård, M. B. Flanagan, I. Lynch, G. Elia and K. Dawson, *ACS Nano*, 2011, **5**, 7503–7509.
27 V. Mirshafiee, M. Mahmoudi, K. Lou, J. Cheng and M. L. Kraft, *Chem. Commun.*, 2013, **49**, 2557–2559.
28 A. Salvati, A. S. Pitek, M. P. Monopoli, K. Prapainop, F. B. Bombelli, D. R. Hristov, P. M. Kelly, C. Åberg, E. Mahon and K. A. Dawson, *Nat. Nanotechnol.*, 2013, **8**, 137–143.
29 Q. Dai, Y. Yan, J. Guo, M. Björnmalm, J. Cui, H. Sun and F. Caruso, *ACS Macro Lett.*, 2015, **4**, 1259–1263.
30 C. H. Dodd, H.-C. Hsu, W.-J. Chu, P. Yang, H.-G. Zhang, J. D. Mountz, K. Zinn, J. Forder, L. Josephson and R. Weissleder, *J. Immunol. Methods*, 2001, **256**, 89–105.
31 P. Nativo, I. A. Prior and M. Brust, *ACS Nano*, 2008, **2**, 1639–1644.
32 S. R. Schwarze, A. Ho, A. Vocero-Akbani and S. F. Dowdy, *Science*, 1999, **285**, 1569–1572.
33 S. Fawell, J. Seery, Y. Daikh, C. Moore, L. L. Chen, B. Pepinsky and J. Barsoum, *Proc. Natl. Acad. Sci. U. S. A.*, 1994, **91**, 664–668.
34 N. Dinauer, S. Balthasar, C. Weber, J. Kreuter, K. Langer and H. von Briesen, *Biomaterials*, 2005, **26**, 5898–5906.
35 S. Venkatesan, J. J. Rose, R. Lodge, P. M. Murphy and J. F. Foley, *Mol. Biol. Cell*, 2003, **14**, 3305–3324.
36 K. Suzuki, S. Hattori, K. Marks, C. Ahlenstiel, Y. Maeda, T. Ishida, M. Millington, M. Boyd, G. Symonds and D. A. Cooper, *Mol. Ther. – Nucleic Acids*, 2013, **2**, e137.
37 K. Suzuki, T. Ishida, M. Yamagishi, C. Ahlenstiel, S. Swaminathan, K. Marks, D. Murray, E. M. McCartney, M. R. Beard and M. Alexander, *RNA Biol.*, 2011, **8**, 1035–1046.
38 N. Archin, A. Liberty, A. Kashuba, S. Choudhary, J. Kuruc, A. Crooks, D. Parker, E. Anderson, M. Kearney and M. Strain, *Nature*, 2012, **487**, 482–485.
39 L. Zhao, A. Seth, N. Wibowo, C.-X. Zhao, N. Mitter, C. Yu and A. P. J. Middelberg, *Vaccine*, 2014, **32**, 327–337.
40 J. Tel, S. P. Sittig, R. A. M. Blom, L. J. Cruz, G. Schreibelt, C. G. Figdor and I. J. M. de Vries, *J. Immunol.*, 2013, **191**, 5005–5012.
41 J. D. Mintern, C. Percival, M. M. J. Kamphuis, W. J. Chin, F. Caruso and A. P. R. Johnston, *Adv. Healthcare Mater.*, 2013, **2**, 940–944.